Electronic Supplementary Material (ESI) for Journal of Materials Chemistry C.

Supporting Information

A Luminescent 2,1,3-Benzoxadiazole-decorated Zirconium-Organic Framework as an Exceptionally Sensitive Turn-On Sensor for Ammonia and Aliphatic Amines in Water

Dmitry I. Pavlov,[a] Taisiya S. Sukhikh,[a] Aleksey A. Ryadun,[a] Vladislava V. Matveevskaya,[a] Konstantin A. Kovalenko,[a] Enrico Benassi,*[b] Vladimir P. Fedin [a] and Andrei S. Potapov*[a]

a. Nikolaev Institute of Inorganic Chemistry, 3 Lavrentiev Ave., 630090 Novosibirsk, Russia, potapov@niic.nsc.ru.

b. Novosibirsk State University, 2 Pirogov Str., 630090 Novosibirsk, Russia, enrico.benassi@outlook.com

Table of Contents

Materials and methods 2
Experimental Procedures 3
Supplementary Figures and Tables 5
References 23

Materials and methods

All of the used reagents were at least of reagent grade and used without additional purification. 4,7-dibromo-2,1,3-benzoxadiazole was synthesized according to the published procedures starting from *o*-nitroaniline[1].

NMR spectra were recorded on Bruker Advance III 500 MHz spectrometer, solvent residual peaks were used as an internal standard.

Thermogravimetric analyses (TGA) were carried out on NETZSCH TG 209 F1 thermobalance. Analysis was conducted in the He atmosphere with heating rate of 10°C·min^{-1}.

Elemental analysis was made on a Vario Microcube analyzer.

Powder X-ray diffraction (PXRD) analysis was performed at room temperature on a Shimadzu XRD-7000 diffractometer (Cu-Kα radiation, λ = 1.54178 Å).

IR spectra in KBr pellets were recorded in the range 4000−400 cm^{-1} on a Bruker Scimitar FTS 2000 spectrometer.

Photoluminescence spectra and luminescence decay kinetics were recorded on Horiba Fluorolog 3 equipped with 450 W ozone-free Xe lamp, a cooled PC177CE-010 photon detection module with R2658 photomultiplier and double grating excitation and emission monochromators. Absolute quantum yields were determined using Quanta-φ integrating sphere. Excitation and emission spectra were corrected for source intensity (lamp and grating) and emission spectral response (detector and grating) by standard correction curves. For measurements powdered samples were placed between two non-fluorescent quartz plates.

Analysis of textural properties was performed by nitrogen adsorption technique at 77 K using Quantochrome's Autosorb iQ instrument. Initially the compound was activated in dynamic vacuum using standard 'outgas' option of the equipment. Nitrogen adsorption−desorption isotherms at 77 K were measured within the range of relative pressures of 10^{-3} to 0.998. The specific surface area was calculated from the data obtained based on the conventional BET model. The framework **UiO-68(bod)** was activated by first exchanging the solvent with chloroform, and then drying on air. 30 mg of the compounds were stirred in 5 mL of chloroform for 24 hours. Suspension was filtered and suspended in fresh chloroform at least three times during this time. Next, the powder was filtered off and dried in oven at 100 °C for 8 hours. Before isotherm measurement, sample was additionally activated and degassed by heating to 100°C in dynamic vacuum.

Experimental Procedures

4,7-di(*p*-carboxymethylphenyl)-2,1,3-benzoxadiazole. 30 mL of DME were added to 100 mL pressure vessel with Teflon screw-cap and bubbled with argon for 30 minutes. 1 g (3.6 mmol) of 4,7-dibromobenzofurazan, 1.64 g (10.8 mmol) of cesium fluoride, 1.31 g (7.92 mmol) of *p*-carboxymethylphenyl boronic acid, and 210 mg (0.18 mmol) of tetrakis(triphenylphosphine)palladium(0) were added to the solution, vessel was tightly capped and heated to 80 °C for 48 hours. After the reaction was complete, the mixture was transferred to the round-bottom flask and evaporated to dryness. Brown-orange solid was suspended in hot chloroform, filtered and the residue was washed with hot chloroform several times. The orange filtrate was evaporated to dryness on a rotary evaporator and the pure product was obtained by recrystallizing the residue from acetone twice. Yield 72 %. Deep-orange needles. $C_{22}H_{16}N_2O_5$ Calc. C, 68.04; H, 4.15; N, 7.21; Found. C, 67.8; H 3.9; N, 7.02. ^{1}H NMR (500 MHz, $CDCl_3$), δ, ppm: 8.17 (AB spin system, J_{AB}=10 Hz, 8H, Ph), 7.78 (s, 2H, benzofurazan), 3.97 (s, 6H, methyl). ^{13}C NMR (125 MHz, $CDCl_3$), δ, ppm: 166.6, 149.0, 139.2, 130.7, 130.2, 129.4, 128.7, 128.4, 52.4. IR, cm^{-1}: 3427, 2945, 1716, 1608, 1433, 1284.

4,7-di(*p*-carboxyphenyl)-2,1,3-benzoxadiazole. 4,7-Di(p-carboxymethylphenyl)-2,1,3-benzoxadiazole (500 mg, 1.39 mmol) of were dissolved in hot MeOH/THF mixture. After complete dissolution, 10 mL of 10 % NaOH were added and the mixture was refluxed for 12 hours. After the hydrolysis was complete, the mixture was evaporated to dryness, residue was dissolved with hot water and greenish-yellow solution was filtered through a glass frit. Concentrated HCl (35 %) was added to the filtrate until the pH value became approximately equal to 4. Bright-yellow precipitate was filtered and dried in oven at 100 °C. Yield 95% Yellow powder. $C_{20}H_{12}N_2O_5$, Calc.: C, 66.67; H, 3.36; N, 7.77; Found: 66.8; H 3.7; N, 7.4. ^{1}H NMR (DMSO-d_6, 400 MHz), δ, ppm: 13.4 (s, 2H, carboxylic H), 8.19 (AB spin system, J_{AB}=8 Hz, 8H, Ph), 8.11 (s, 2H, benzofurazan). ^{13}C NMR (DMSO-d_6, 100 MHz), δ, ppm: 167.3, 149.1, 138.9, 131.7, 131.1, 130.3, 128.8, 127.7.

Sample containing 1% of 2,1,3-benzoxadiazole ligand. 7 mg (0.03 mmol) of $ZrCl_4$ and 107 mg (0.87 mmol) of benzoic acid were dissolved in 2 mL of DMF in 4 mL screwcap glass vial and incubated at 80°C for 1 hour. Then, 10 mg (0.029 mmol) of 2',5'-dimethyl-[1,1':4',1''-terphenyl]-4,4''-dicarboxylic acid and 0.1 mg of 4,7-di(carboxyphenyl)-2,1,3-benzoxadiazole (as 0.1 mL of DMF solution with concentration of 5 mg/mL) were added. Vial was heated in isothermal oven at 120°C for 48 hours. White microcrystalline precipitate was collected by filtration, washed with fresh DMF followed by ethanol and dried in air.

Sample containing 10% of 2,1,3-benzoxadiazole ligand. 7.5 mg (0.032 mmol) of $ZrCl_4$ and 120 mg (0.96 mmol) of benzoic acid were dissolved in 1 mL of DMF in 4 mL screwcap glass vial and incubated at 80°C for 1 hour. Then, 10 mg (0.029 mmol) of 2',5'-dimethyl-[1,1':4',1''-terphenyl]-4,4''-dicarboxylic acid and 1

mg of 4,7-di(carboxyphenyl)-2,1,3-benzoxadiazole (as 1 mL of DMF solution with concentration of 5 mg/mL) were added. Vial was heated in isothermal oven at 120°C for 48 hours. Greenish-white microcrystalline precipitate was collected by filtration, washed with fresh DMF followed by ethanol and dried in air.

Defect quantification. Defect quantification was performed by NMR analysis of the digested MOF samples with the internal standard (hexamethylbenzene). For the activated ideal UiO-68(bod) containing six linkers per one zirconium cluster the formula is $C_{120}H_{60}N_{12}O_{30}Zr_6(OH)_4O_4$. This results in the roughly 1:3 (75,4 mass % of the organic part) mass ratio of the inorganic and organic parts, respectively. By comparing the integral intensity of the ligand signals in the NMR spectrum with the internal standard, the ligand mass in the sample taken for digestion may be calculated. Comparing the experimental result with the calculated ratio for the ideal sample allows to evaluate the defect content. Results are presented in Table S1.

MOF digestion. A solution of hexamethylbenzene in DMSO-d_6 with concentration of 1.4 $mg \cdot mL^{-1}$ was prepared. To this, several drops of D_2SO_4 were added. Solution (700 µl) was added to the sample in 4 mL vial, which was capped and heated at 100°C for 10 minutes. Clear solutions were transeffered to the NMR tubes and subjected to analysis.

Test paper preparation. Fluorescent test paper was prepared by immersing the filter paper in the EtOH suspension (40 mg in 20 mL) of MOF in ultrasonic bath for 2 hours. Then, the capillary was used to absorb DEA solution to write the symbols on the test paper. The results demonstrate increasing of fluorescence intensity under UV light (Fig. 6, main article). Therefore, the test paper provides an expedite and naked-eye recognizable method for the detection of amines.

Model wastewater preparation. An aqueous solution was prepared using 1 L of distilled water, 80 mg of $CaCl_2$, 30 mg of $Mg(NO_3)_2$, 20 mg of K_2SO_4, 60 mg of Na_2SO_4 and used for preparation of the suspension.

Supplementary Figures and Tables

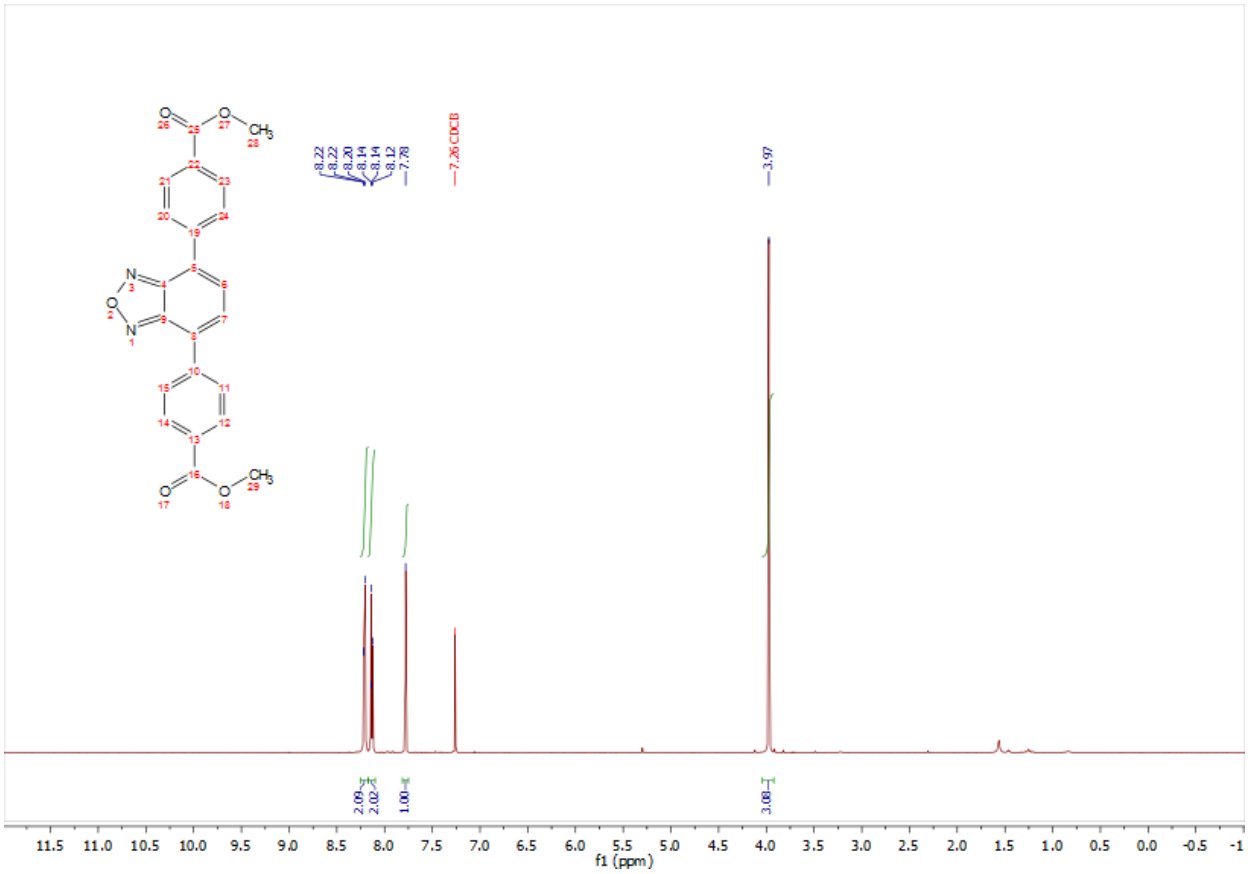

Figure S1. NMR ^{1}H spectrum of 4,7-di(p-carboxymethylphenyl)-2,1,3-benzoxadiazole in $CDCl_3$.

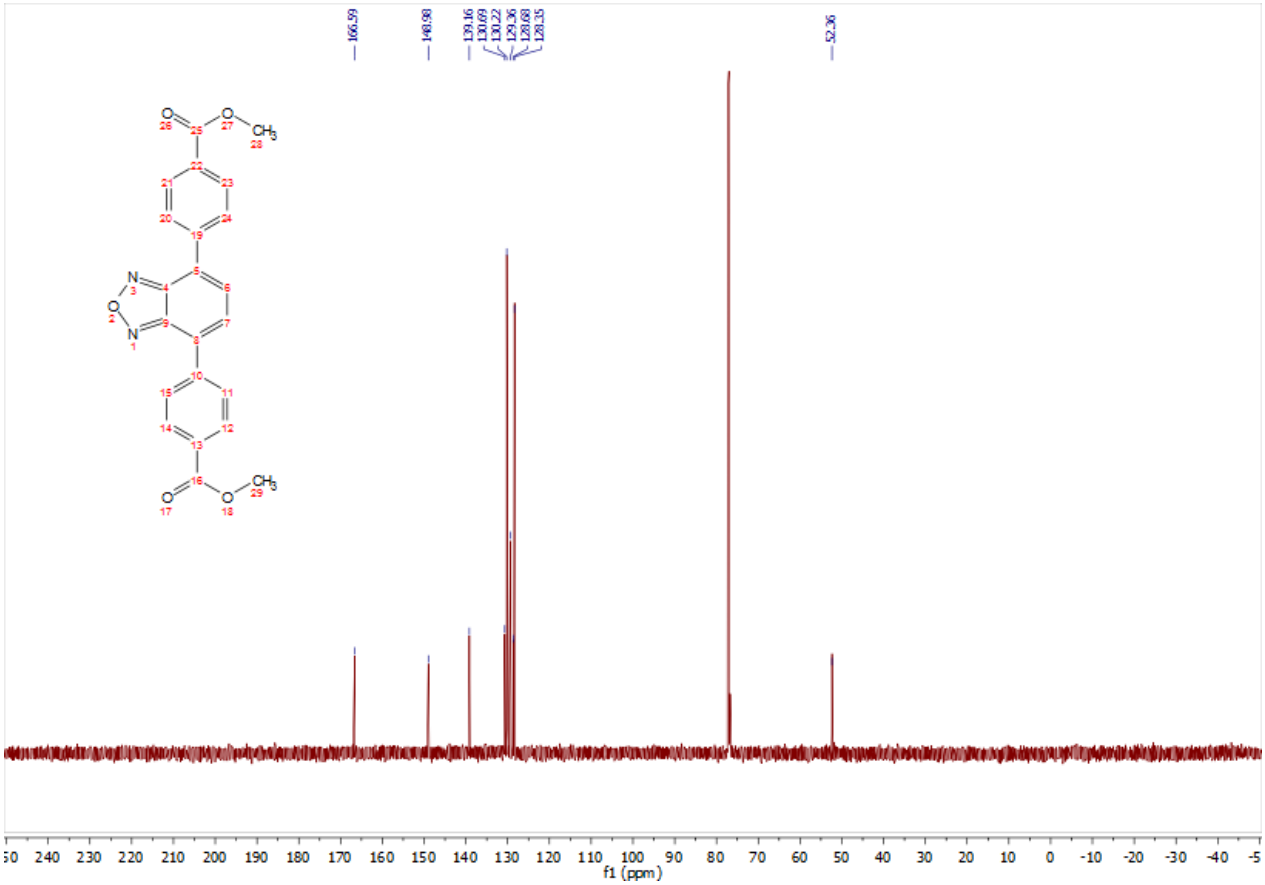

Figure S2. NMR ^{13}C spectrum of 4,7-di(p-carboxymethylphenyl)-2,1,3-benzoxadiazole in $CDCl_3$.

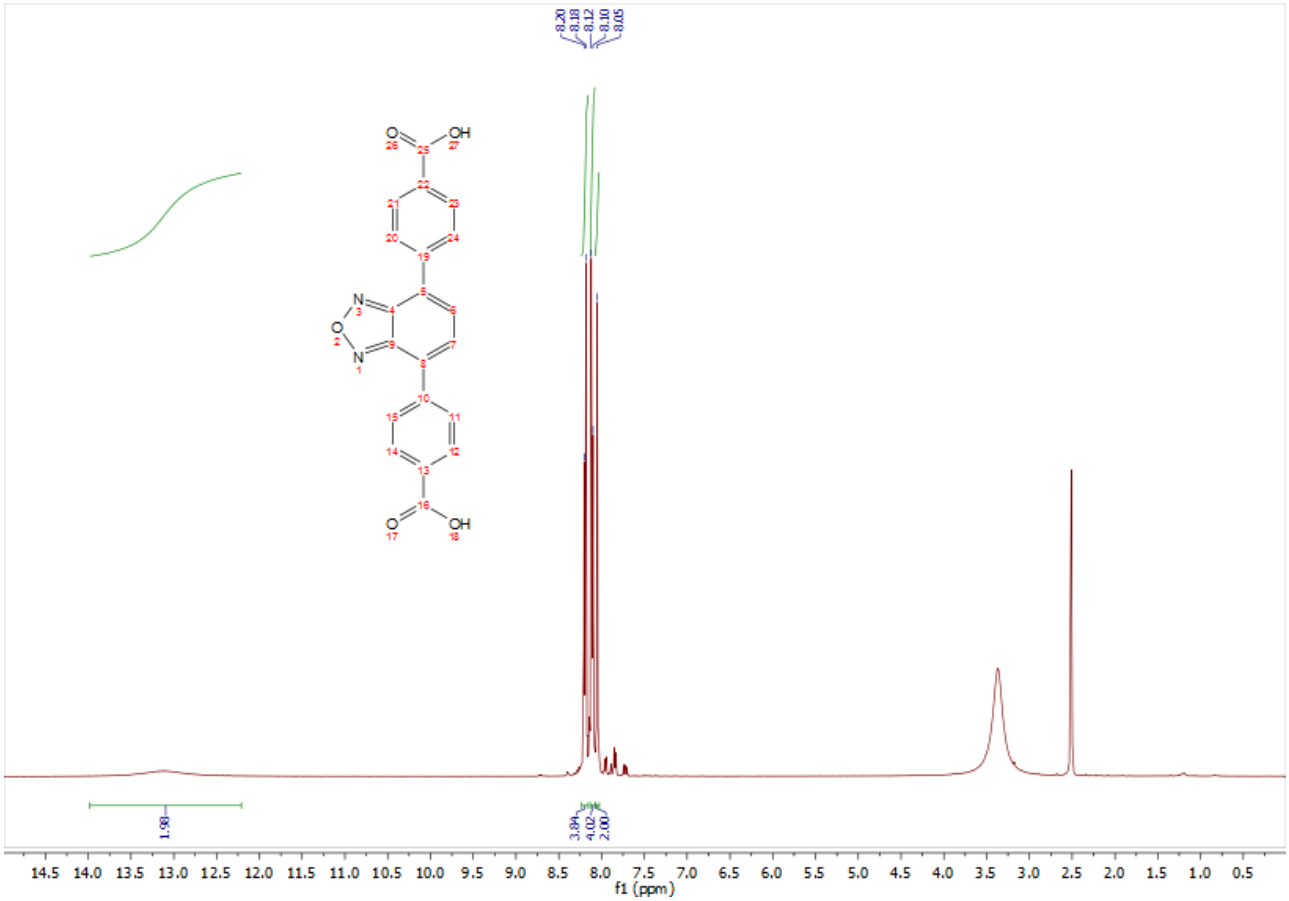

Figure S3. NMR ^{1}H spectrum of 4,7-di(p-carboxyphenyl)-2,1,3-benzoxadiazole in DMSO-d_6.

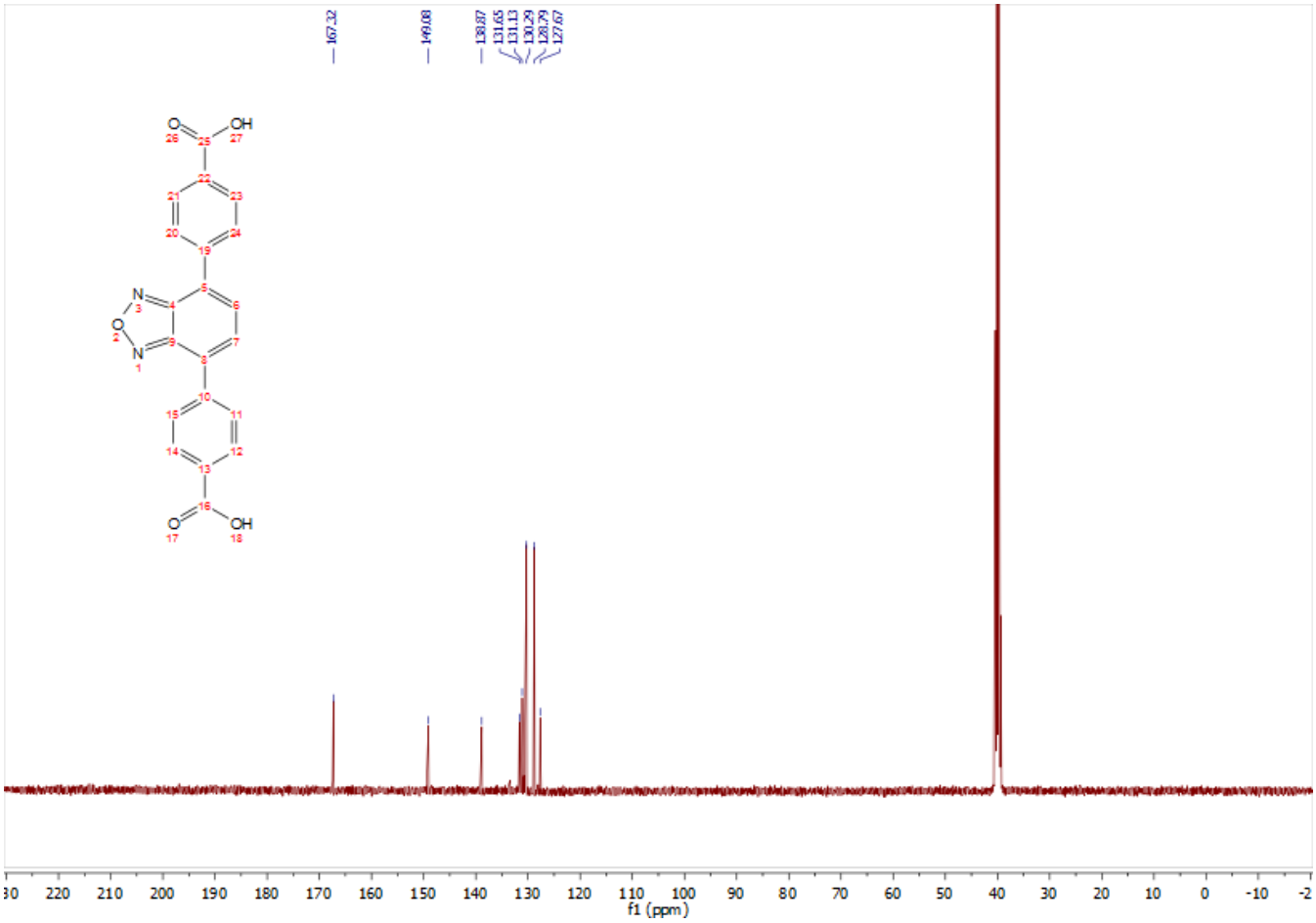

Figure S4. NMR ^{13}C spectrum of 4,7-di(p-carboxyphenyl)-2,1,3-benzoxadiazole in DMSO-d_6.

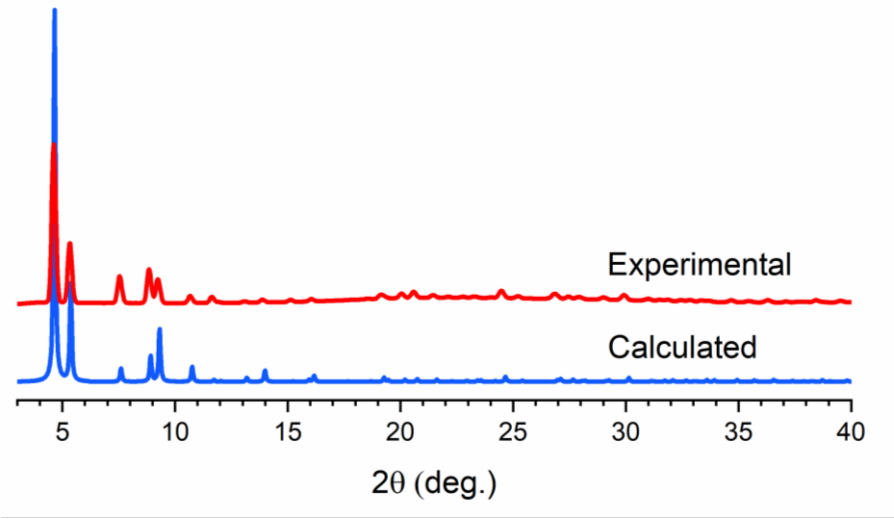

Figure S5. Calculated and experimental PXRD patterns of **UiO-68(bod)**.

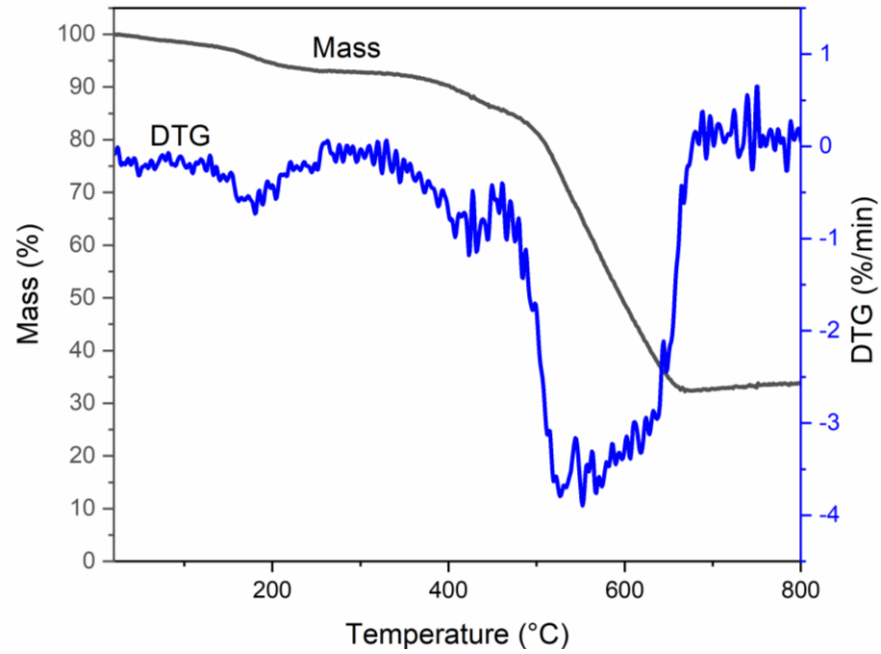

Figure S6. TGA diagram of activated **UiO-68(bod)**.

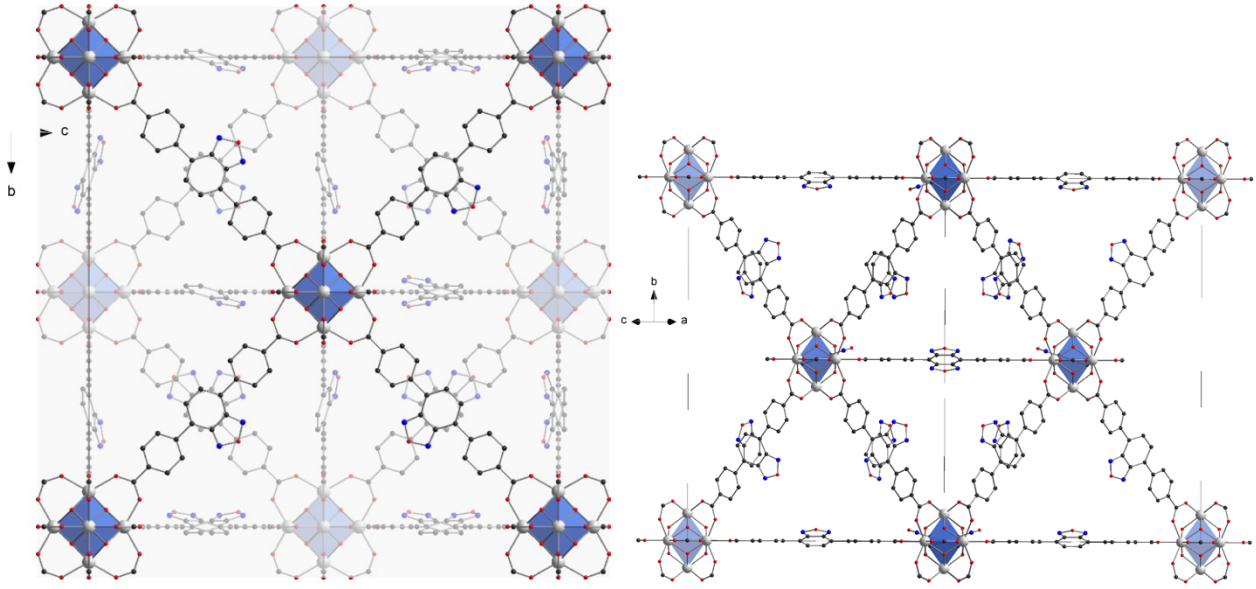

Figure S7. Crystal structure of **UiO-68(bod)** according to single crystal X-ray diffraction analysis.

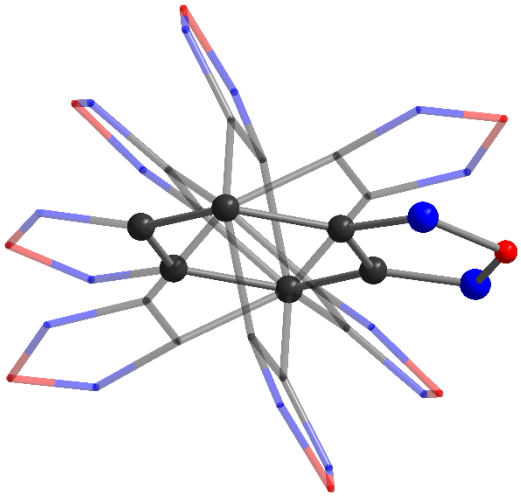

Figure S8. Disorder of 2,1,3-benzoxadiazole moiety over 8 positions.

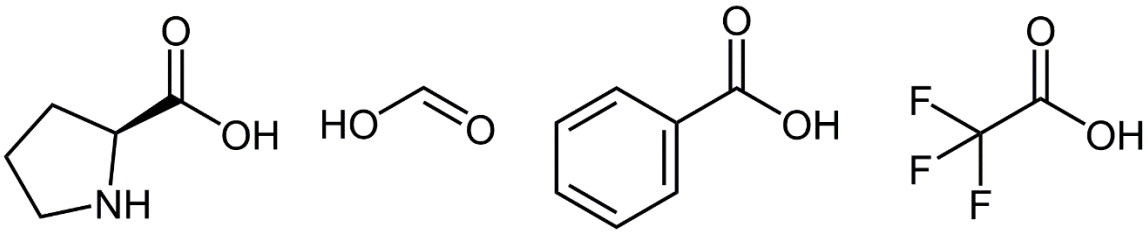

Figure S9. Modulators tested in the synthesis of **UiO-68(bod)**. Left to right: L-proline, formic acid, benzoic acid, trifluoroacetic acid.

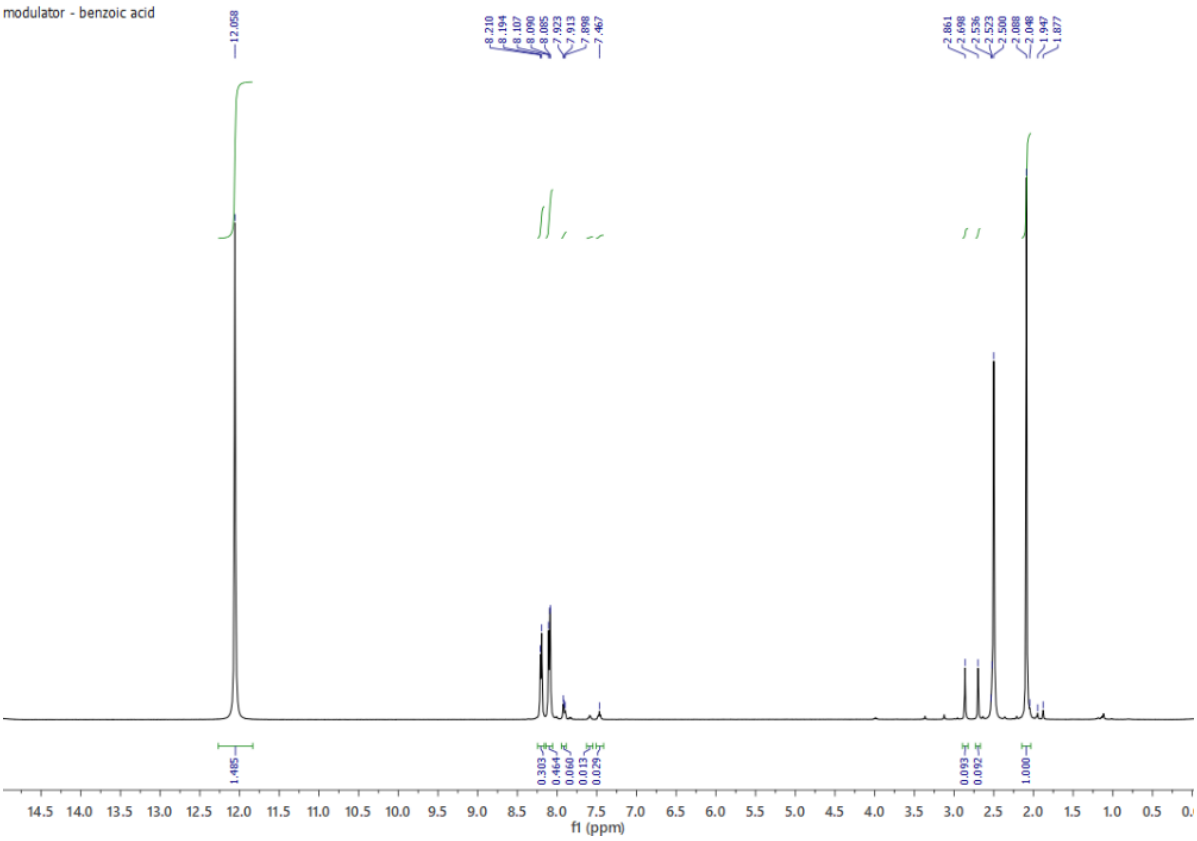

Figure S10. ^{1}H NMR of **UiO-68(bod)** sample obtained with the use of benzoic acid as a modulator.

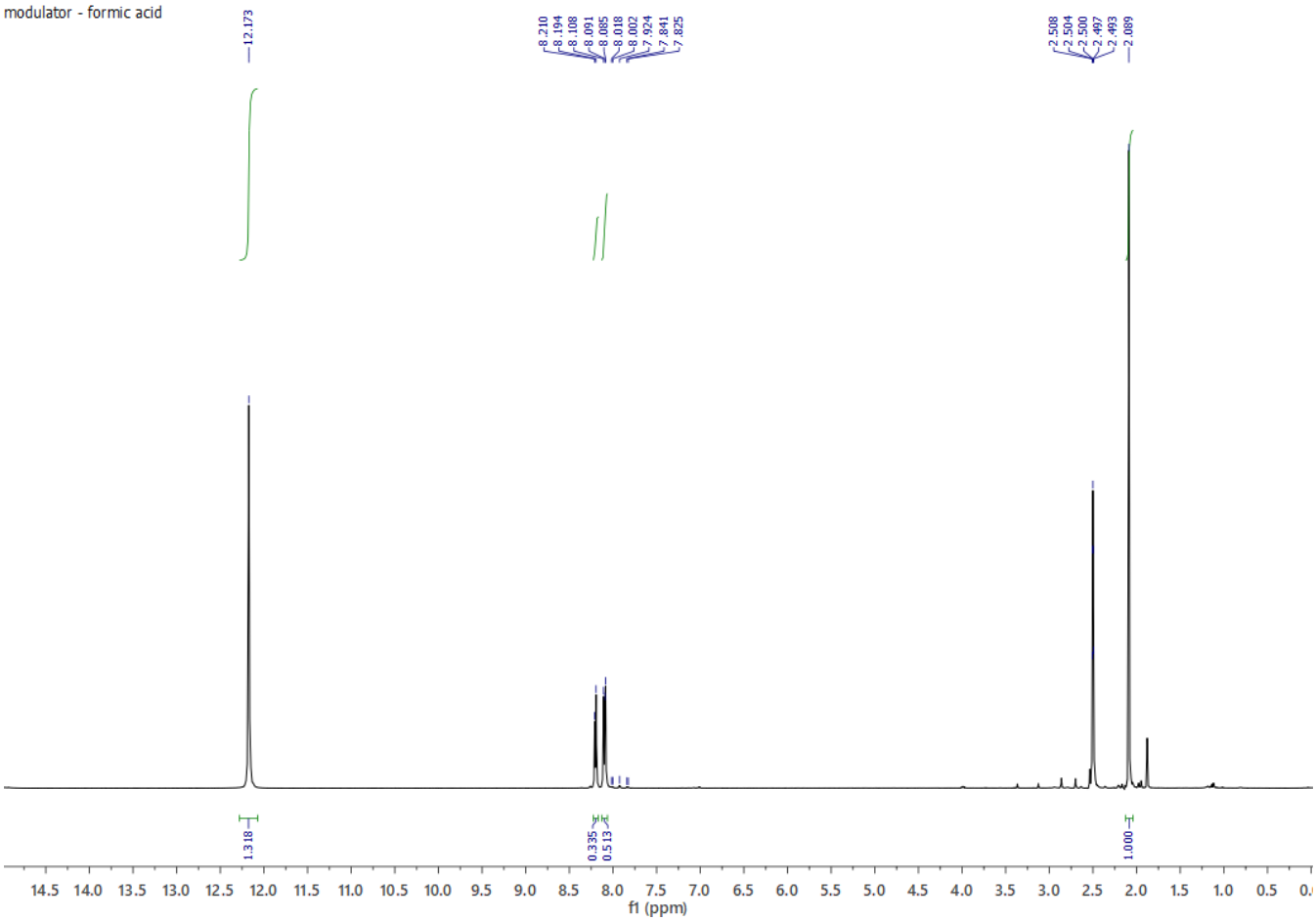

Figure S11. ^{1}H NMR of **UiO-68(bod)** sample obtained with the use of formic acid as a modulator.

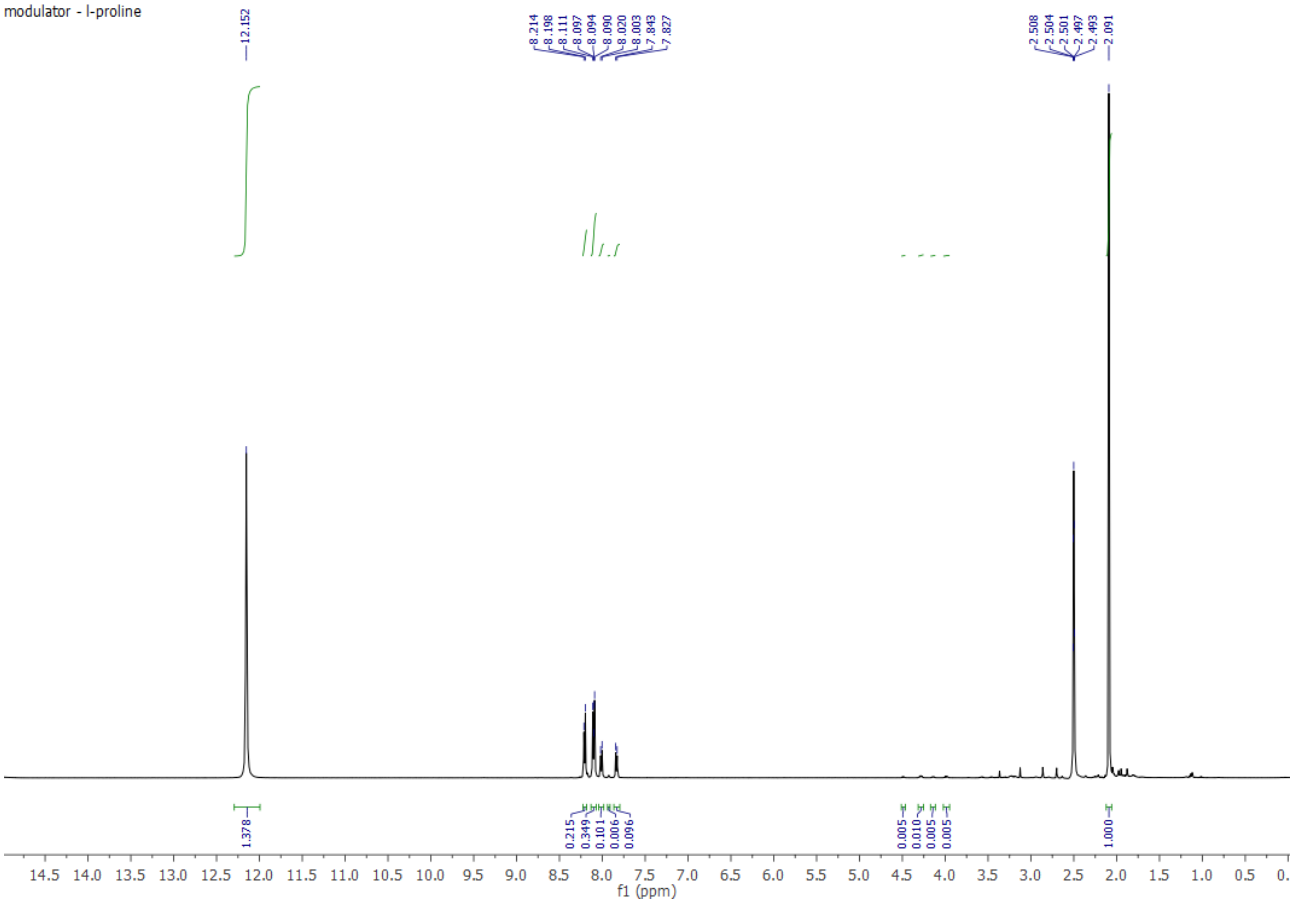

Figure S12. ^{1}H NMR of **UiO-68(bod)** sample obtained with the use of *L*-proline as a modulator.

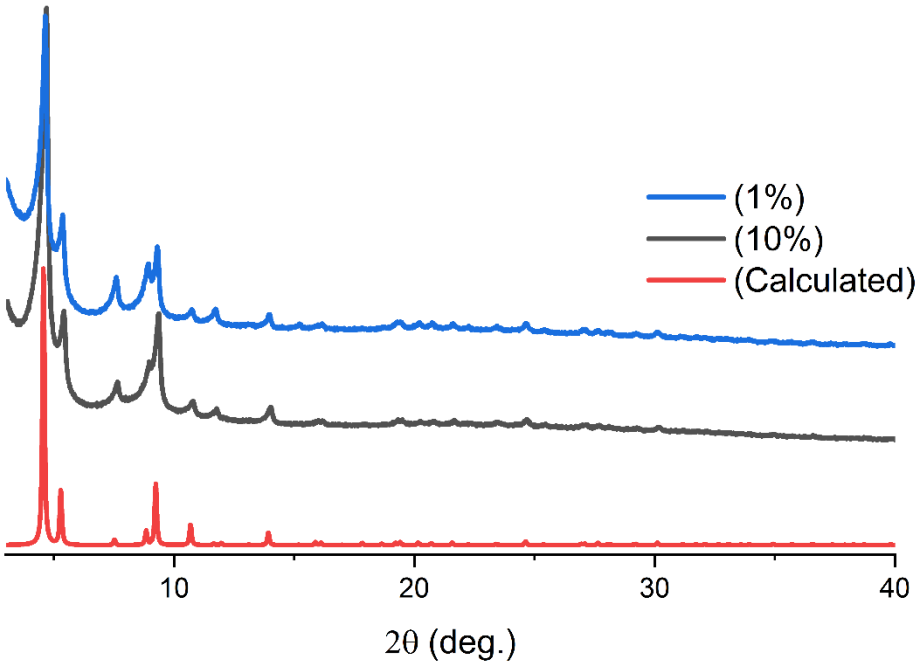

Figure S14. PXRD patterns of mixed-ligand frameworks. Percentage in parentheses refer to 4,7-di(carboxyphenyl)-2,1,3-benzoxadiazole content.

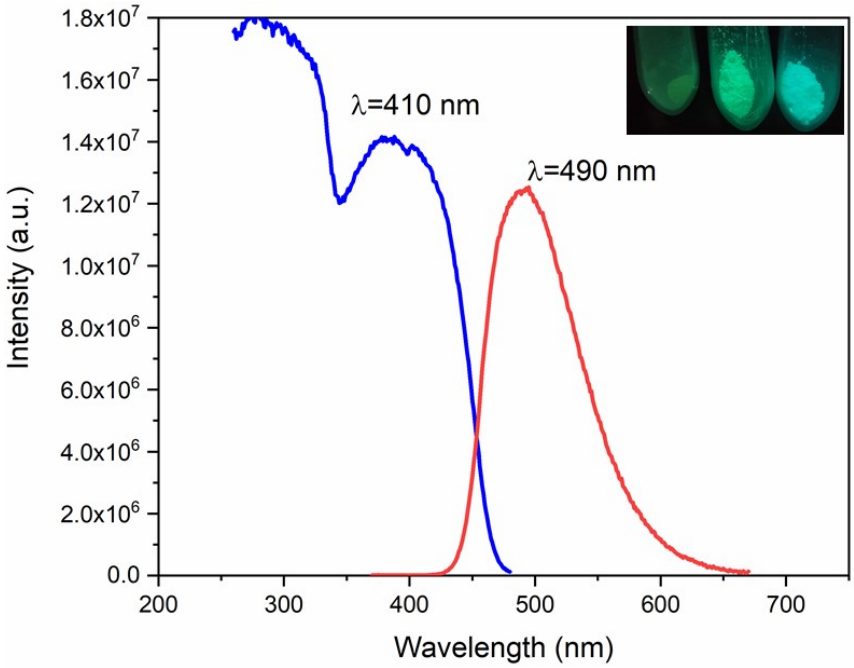

Figure S15. Excitation (blue line) and emission (red line) spectra of PCN-57 with 1% 4,7-di(p-carboxyphenyl)-2,1,3-benzoxadiazole ligand. Inset – optical photograph of the luminescence of, left to right: pristine UiO-68(bod), 10% bod PCN-57 and 1% bod PCN-57.

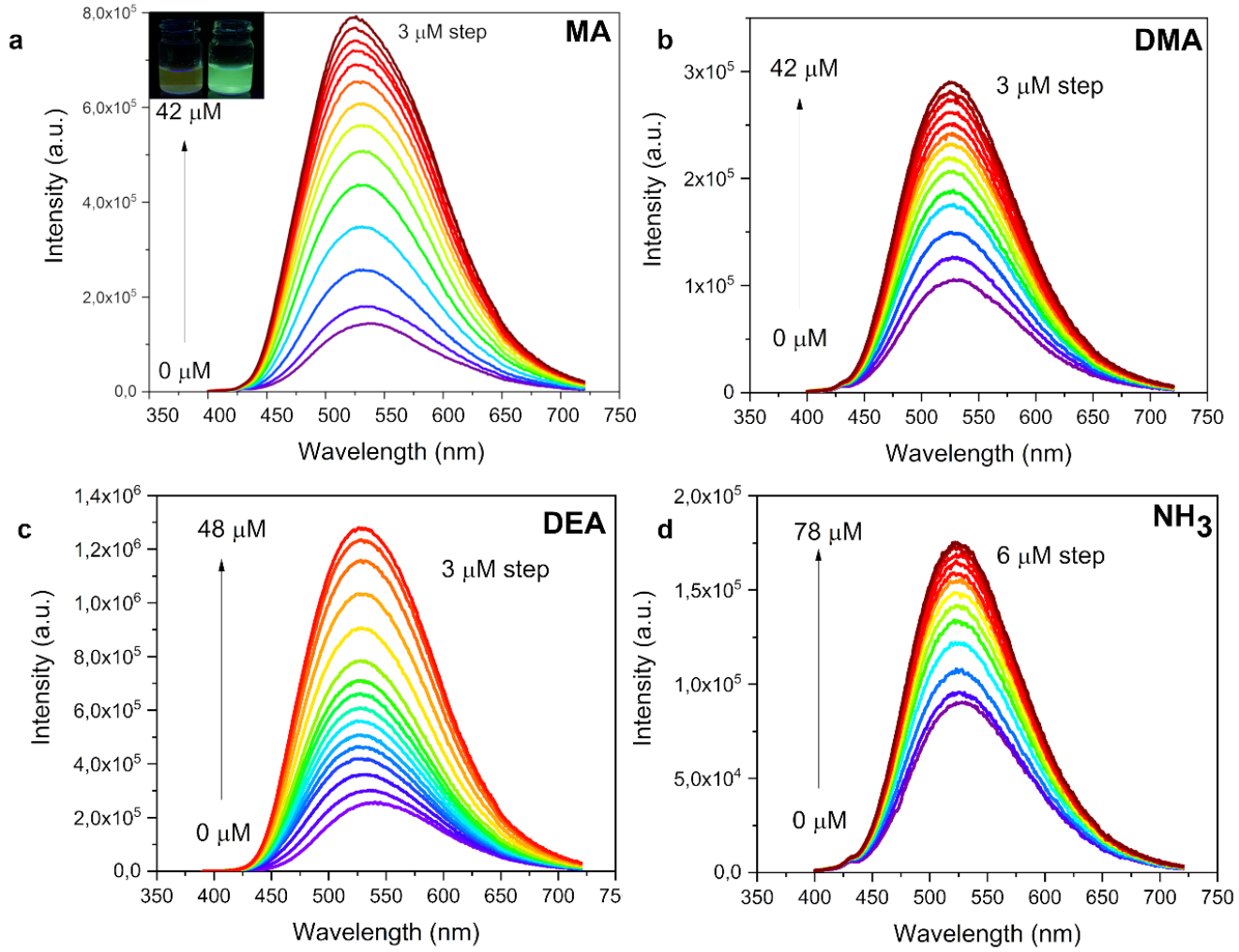

Figure S16. Photoluminescence spectra of the **UiO-68(bod)** upon a gradual increase of MA (a), DMA (b), DEA (c) or NH_3 (d) concentration. Inset to panel a – a photograph of the change in luminescence of the suspension upon addition of MA.

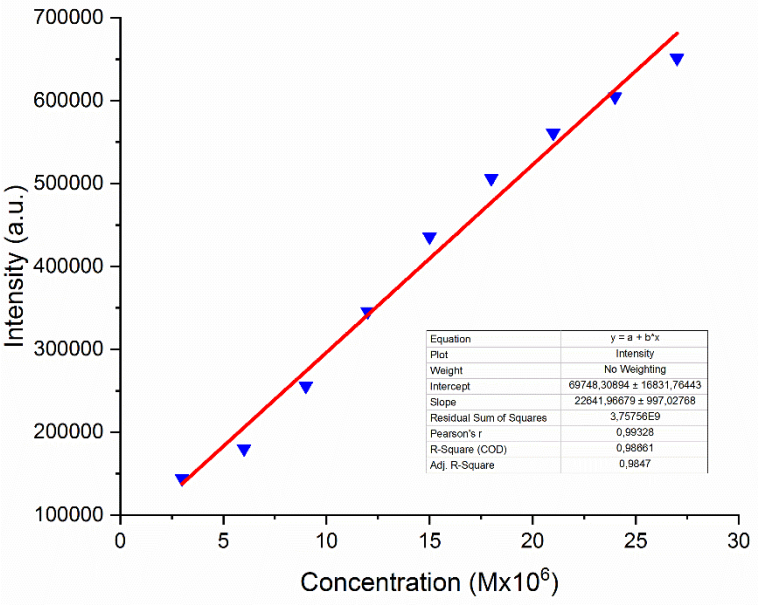

Figure S17. Linear fit for the methylamine concentration-intensity correlation.

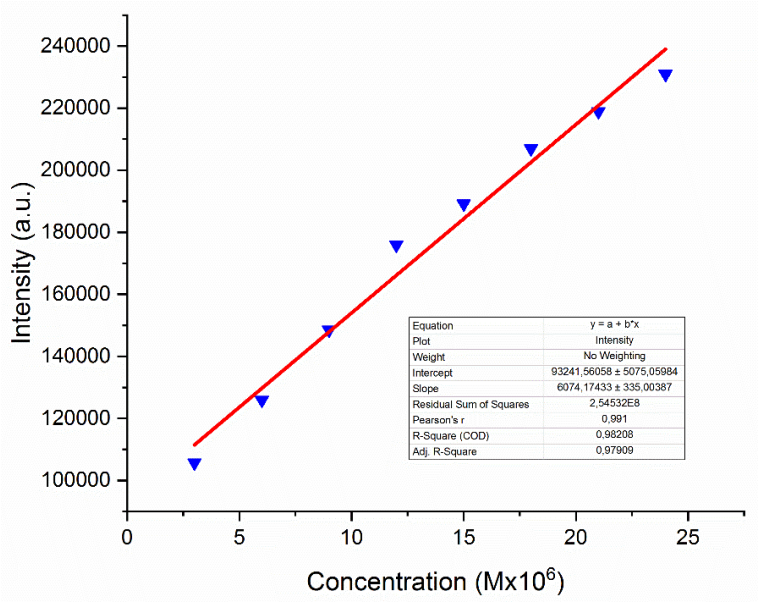

Figure S18. Linear fit for the dimethylamine concentration-intensity correlation.

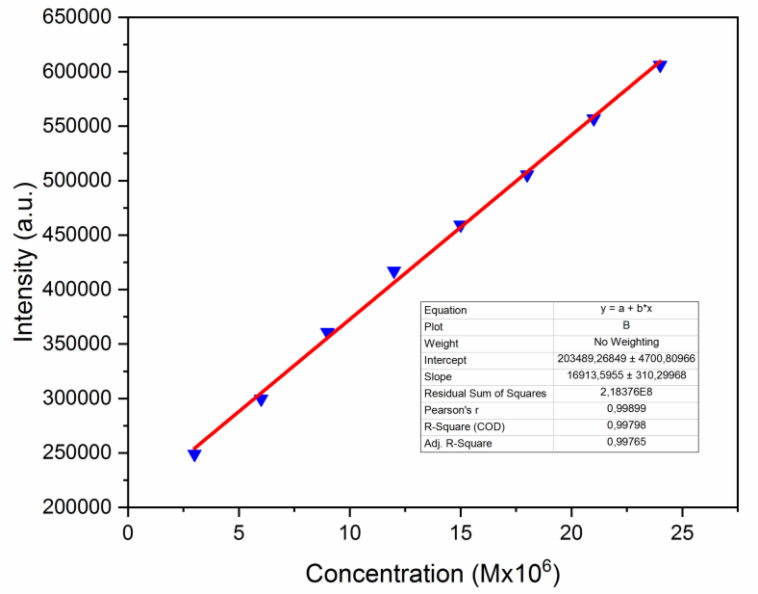

Figure S19. Linear fit for the diethylamine concentration-intensity correlation.

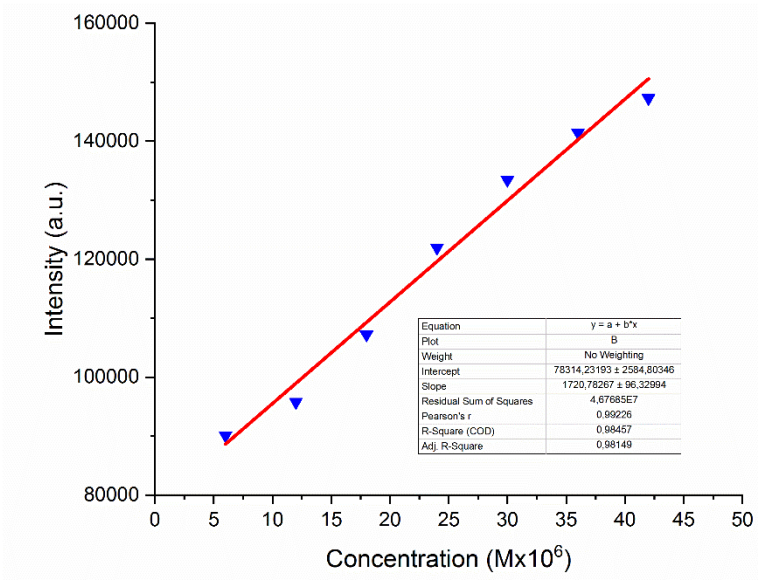

Figure S20. Linear fit for the ammonia concentration-intensity correlation.

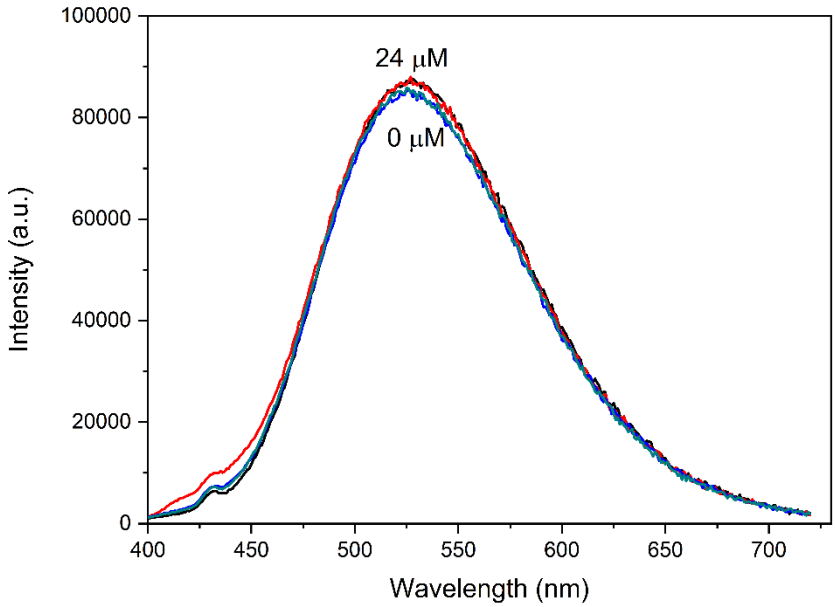

Figure S21. Dependence of the luminescence intensity of **UiO-68(bod)** aqueous suspension on the addition of aniline. No change is observed.

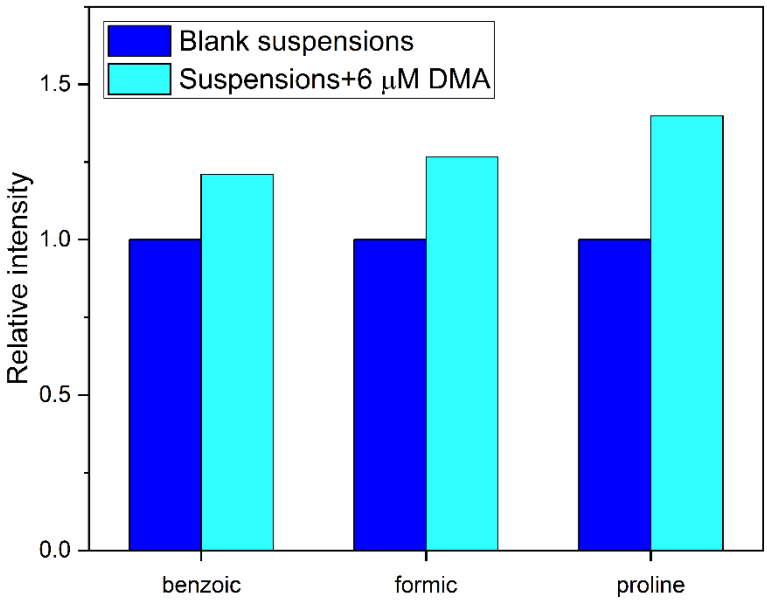

Figure S22. Comparison of the luminescence response of the materials obtained with the use of different modulators.

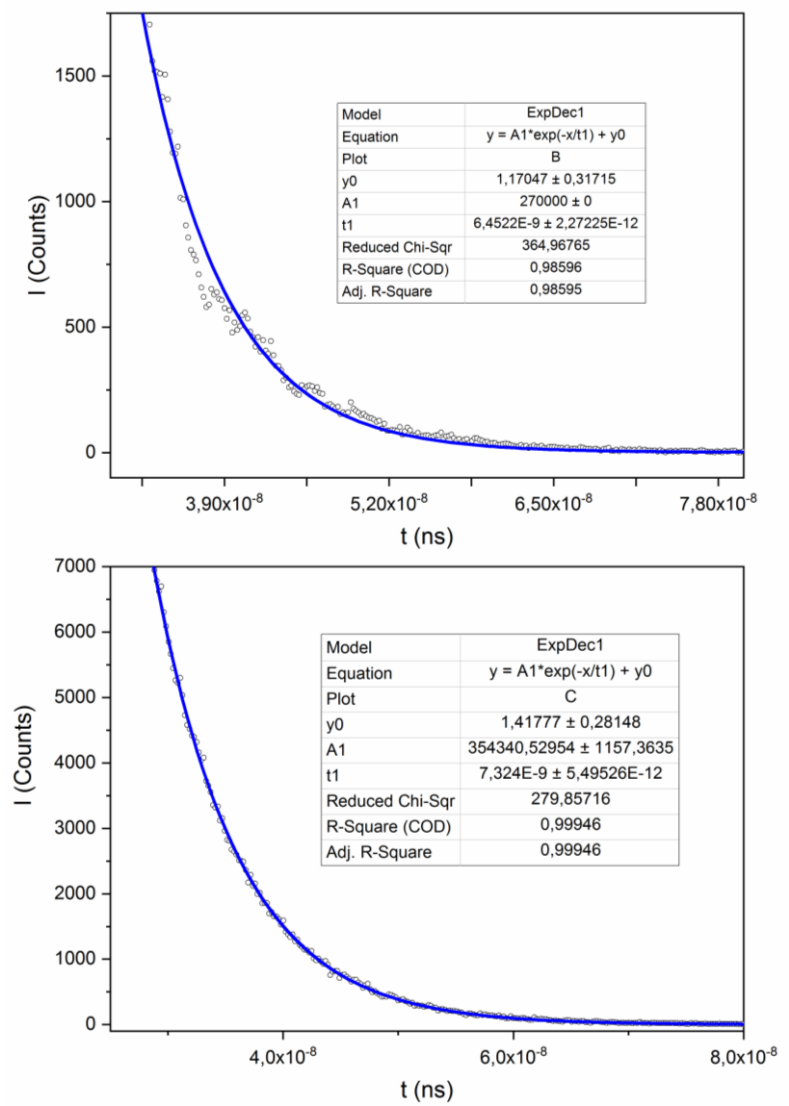

Figure S23. Fluorescence decay curves of pristine **UiO-68(bod)** (bottom) and **UiO-68(bod)** in presence of dimethylamine (top).

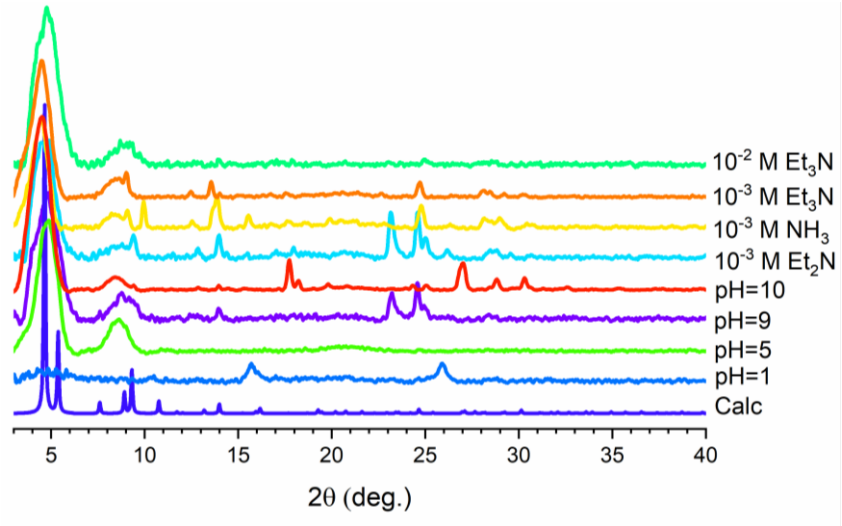

Figure S24. PXRD patterns of **UiO-68(bod)** samples after soaking in different solutions for 24 hours.

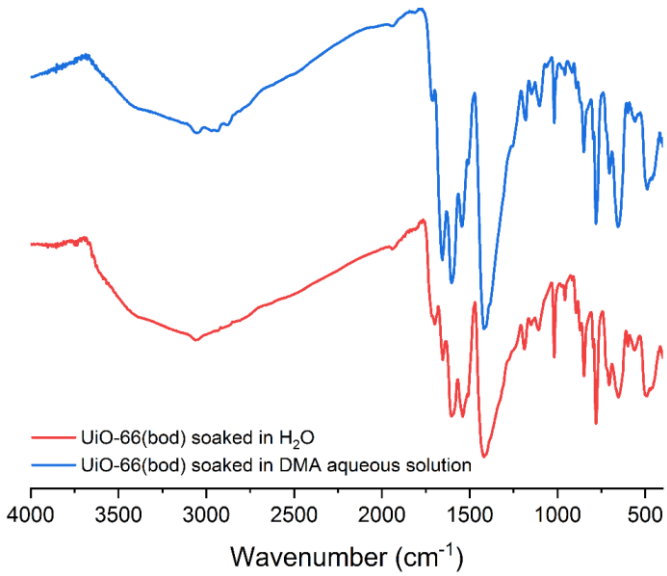

Figure S25. IR spectra of **Ui-68(bod)** samples after soaking in water and DMA aqueous solution (1·mM).

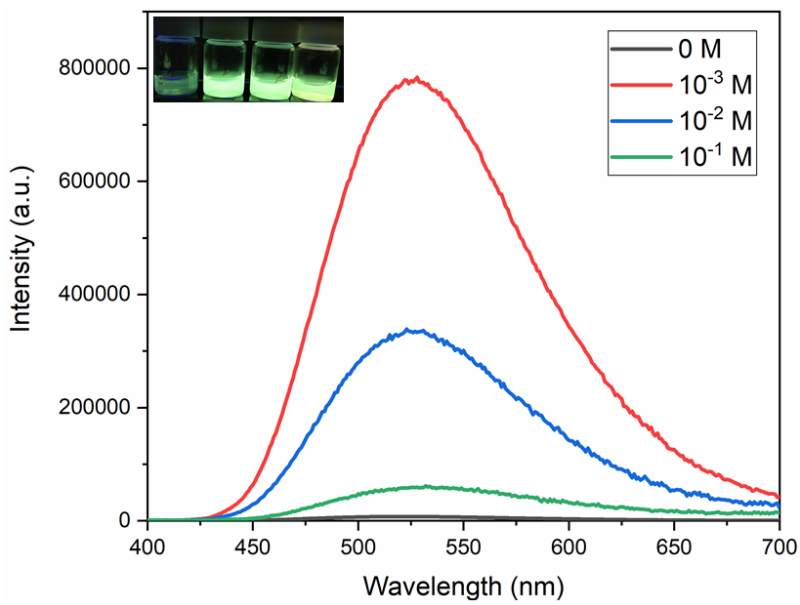

Figure S26. Luminescence spectra of the **UiO-68(bod)** aqueous suspension at high diethylamine concentrations. Inset – optical photograph of the suspensions, left to right: blank, 10^{-3} M, 10^{-2} M, 10^{-1} M.

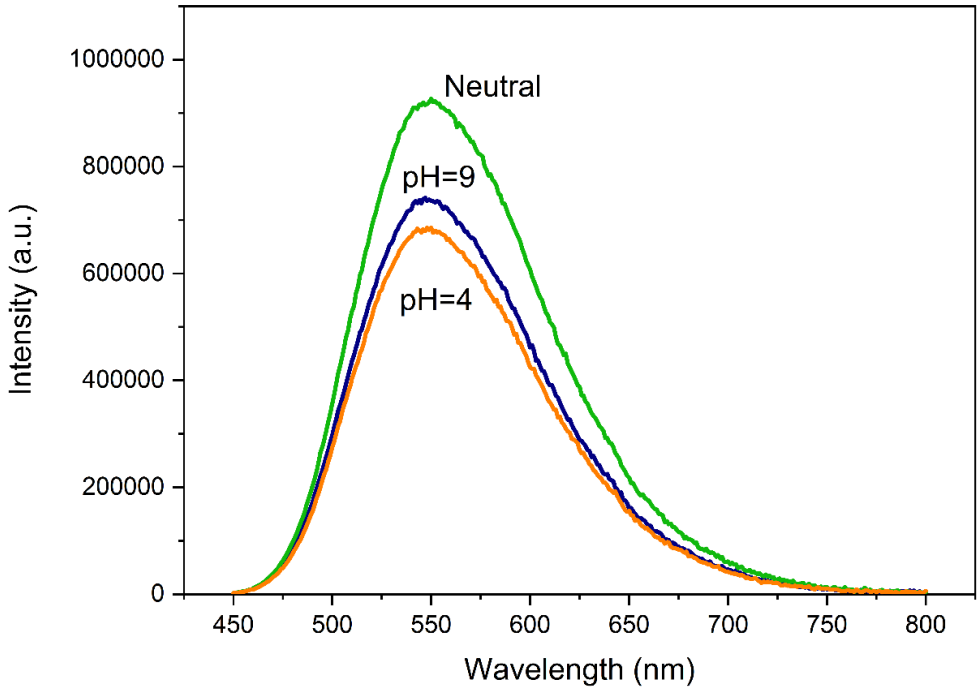

Figure S27. Luminescence spectra of aqueous **UiO-68(bod)** suspension at different pH values.

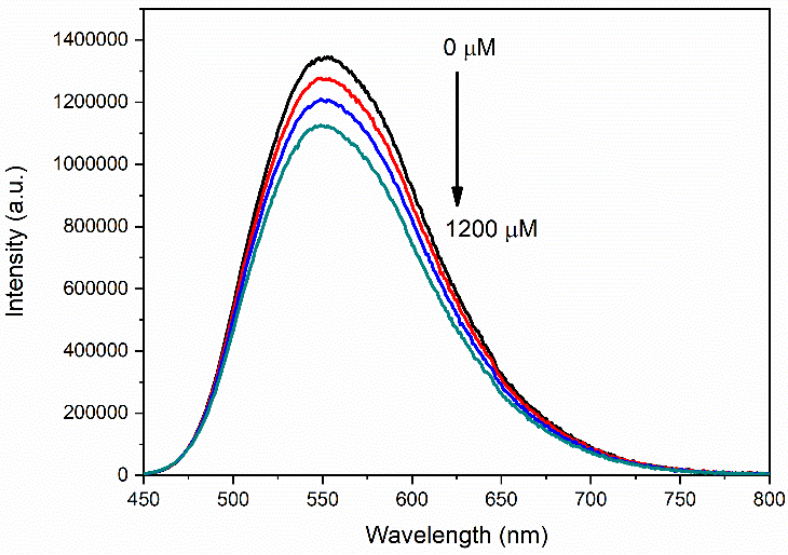

Figure S28. Luminescence spectra of **UiO-68(bod)** suspension with gradual addition of dimethylamine hydrochloride.

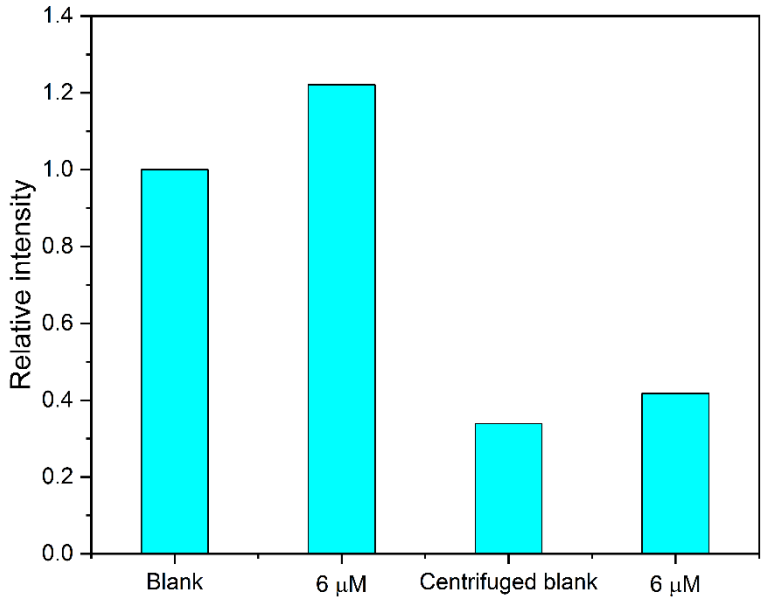

Figure S29. Luminescence intensity of **UiO-68(bod)** in the cycling experiment. Intensity change expressed as $(I-I_0)/I_0$ in both cases is equal to 0.24.

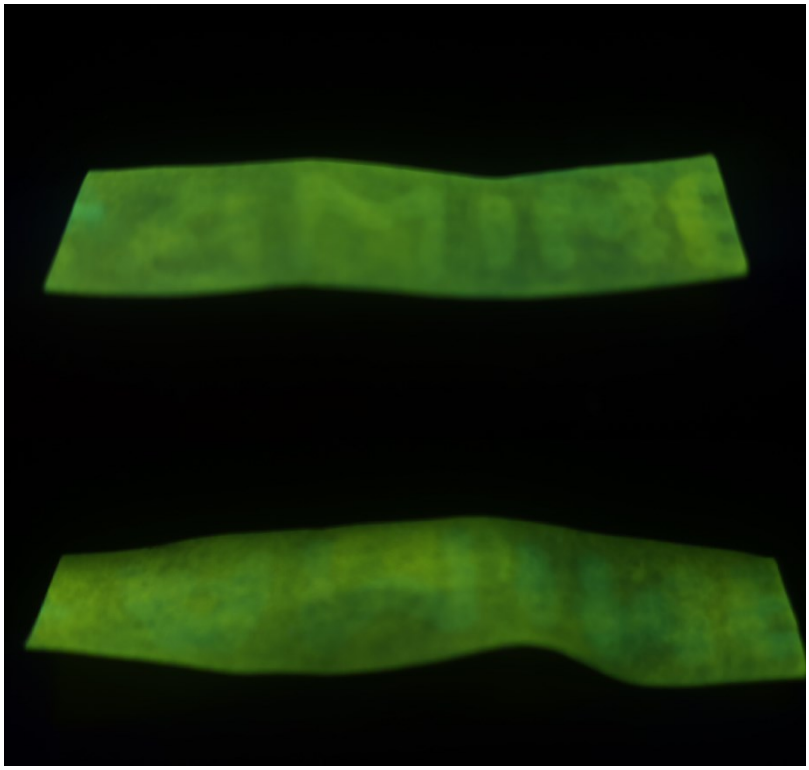

Figure S30. Test-paper with the adsorbed amine solution (word “AMINE” written) before (top) and after (bottom) heating at 60°C for 15 minutes.

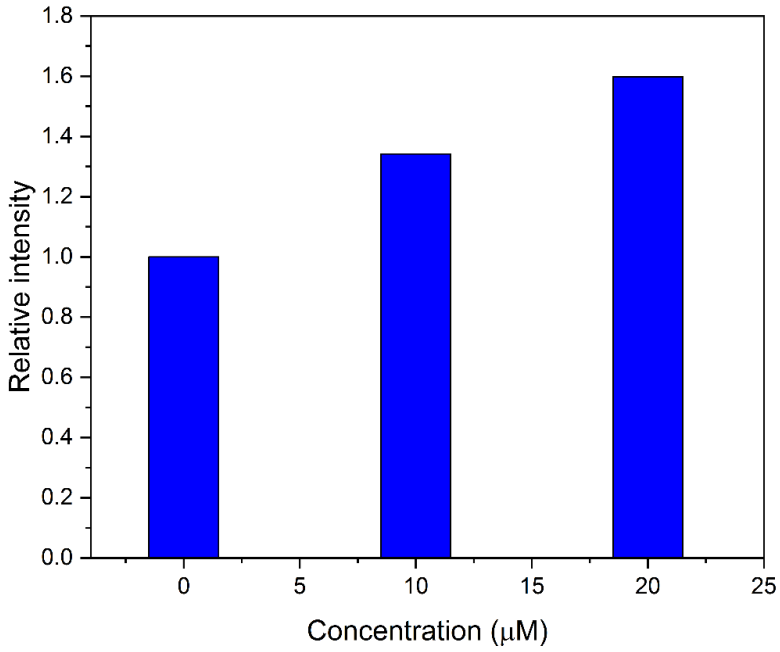

Figure S31. Results of the luminescence sensing experiment with model contaminated wastewater. Intensity of the blank suspension and 10 μM DMA solution were recorded. Then, another 10 μM DMA were added. Calculated total concentration from the increase in intensity was 17 μM, giving recovery of 85 %.

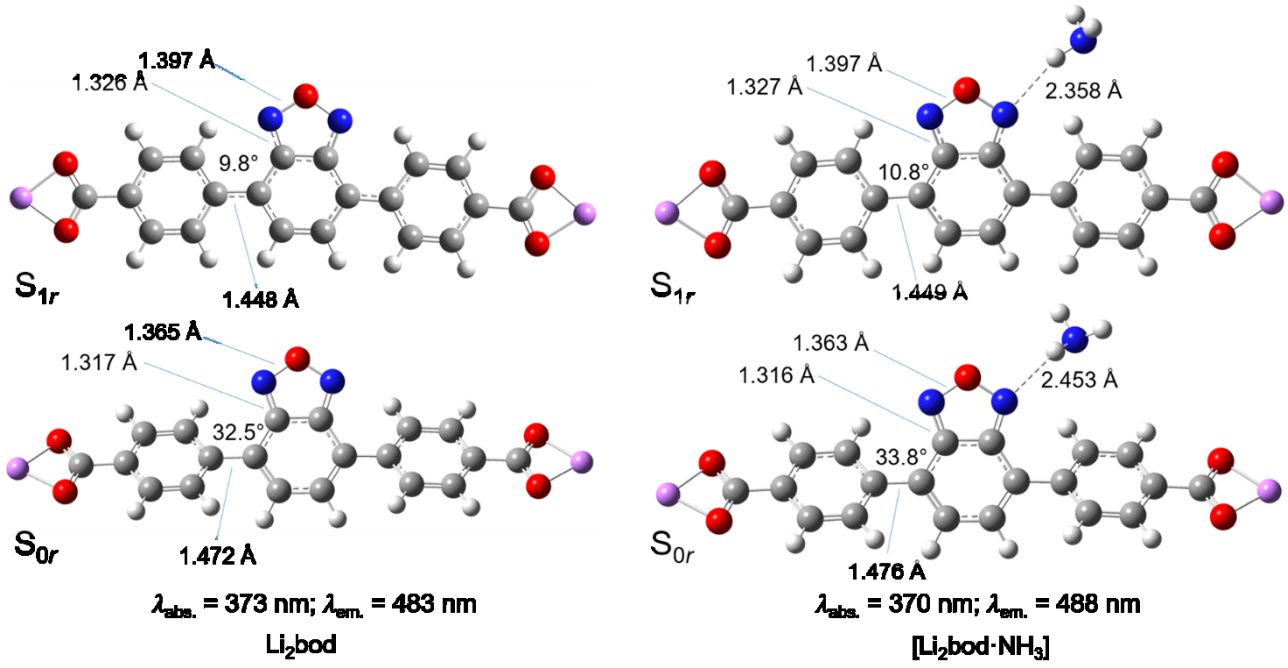

Figure S32. Optimised ground and excited state geometries (DFT B3LYP 6-311+G(2d,p)) of the UiO-68(**bod**) linker model (left, Li_2bod) and its NH_3 adduct (right, $[Li_2bod{\cdot}NH_3]$) with selected geometrical parameters. Absorption and fluorescence maximum wavelengths, calculated at TD-DFT CAM-B3LYP aug-cc-pVTZ level of theory, are also depicted. Legend of colours: white (H), grey (C), blue (N) and red (O).

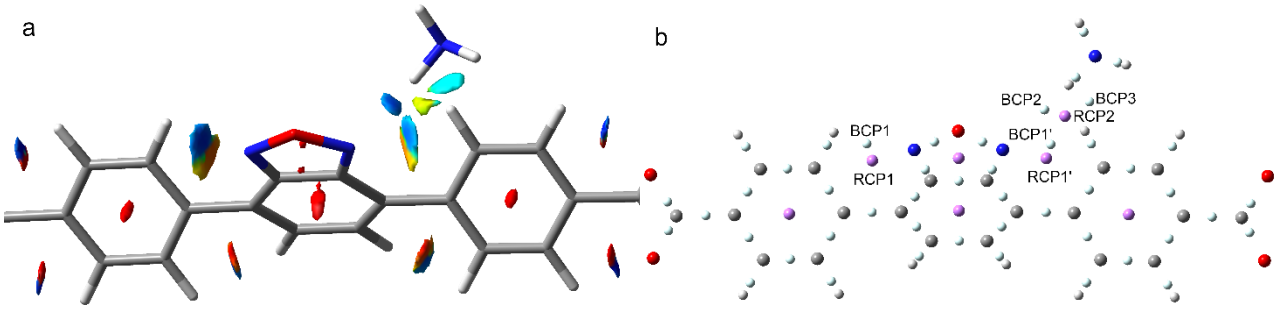

Figure S33. Plot of the (a) Reduced Density Gradient (RDG) isosurfaces (isovalue s = ½) and (b) the Critical Points (CPs). Colour scale: -0.012 a.u. (blue; strong attraction) ≤ sign(λ_2)ρ(**r**) ≤ +0. 012 a.u. (red; strong repulsion). Legend of colours of CPs: light blue (Bond CPs), and mauve (Ring CPs).

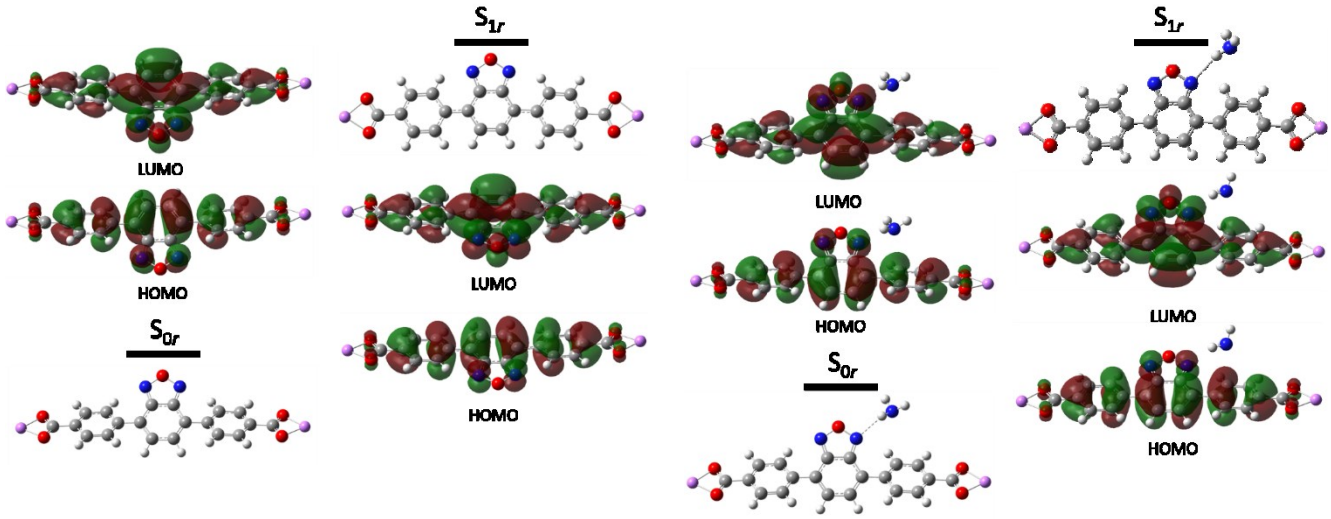

Figure S34. Frontier molecular orbitals (CAM-B3LYP aug-cc-pVTZ) of relaxed ground and excited singlet states (B3LYP 6-311+G(2d,p)) of Li_2bod and Li_2bod-NH_3. MO surfaces are shown for 0.02 e/Bohr^3 isovalues.

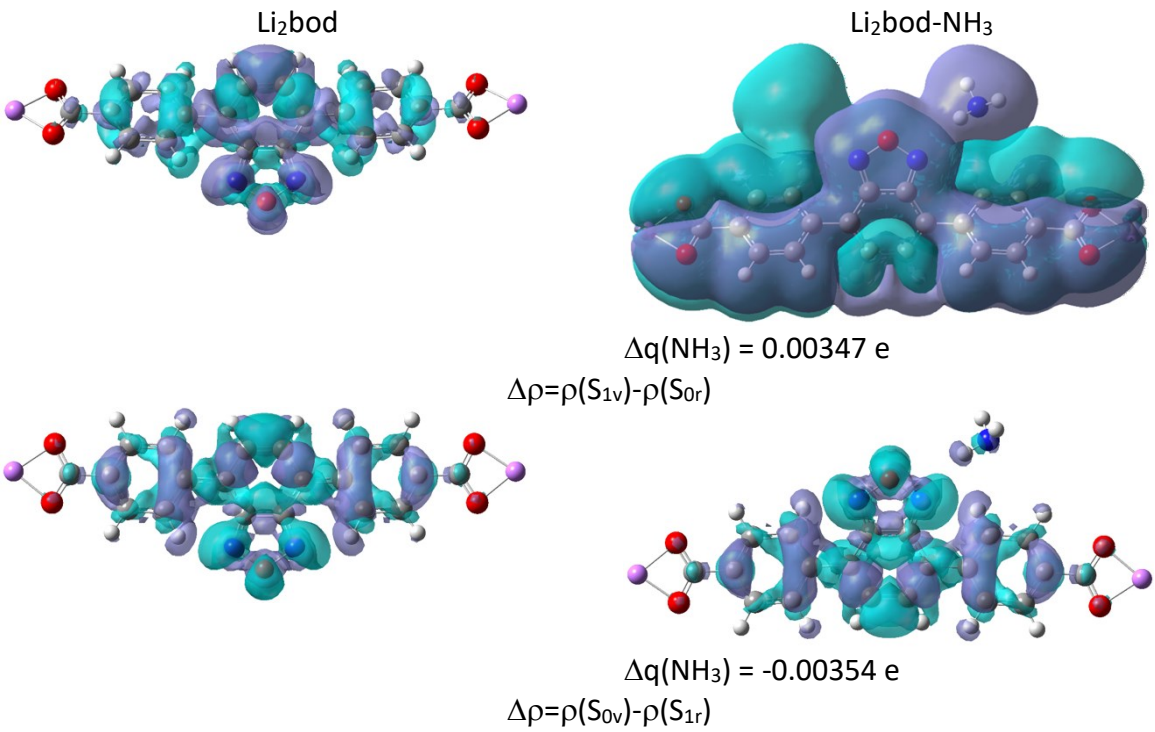

Figure S35. Isosurfaces (0.0004 $e^{1/2}/Bohr^{3/2}$) of electron density difference and changes of the sum of ESP atomic charges on NH_3 molecule for absorption and emission processes of Li_2bod and Li_2bod-NH_3 calculated CAM-B3LYP aug-cc-pVTZ level of theory.

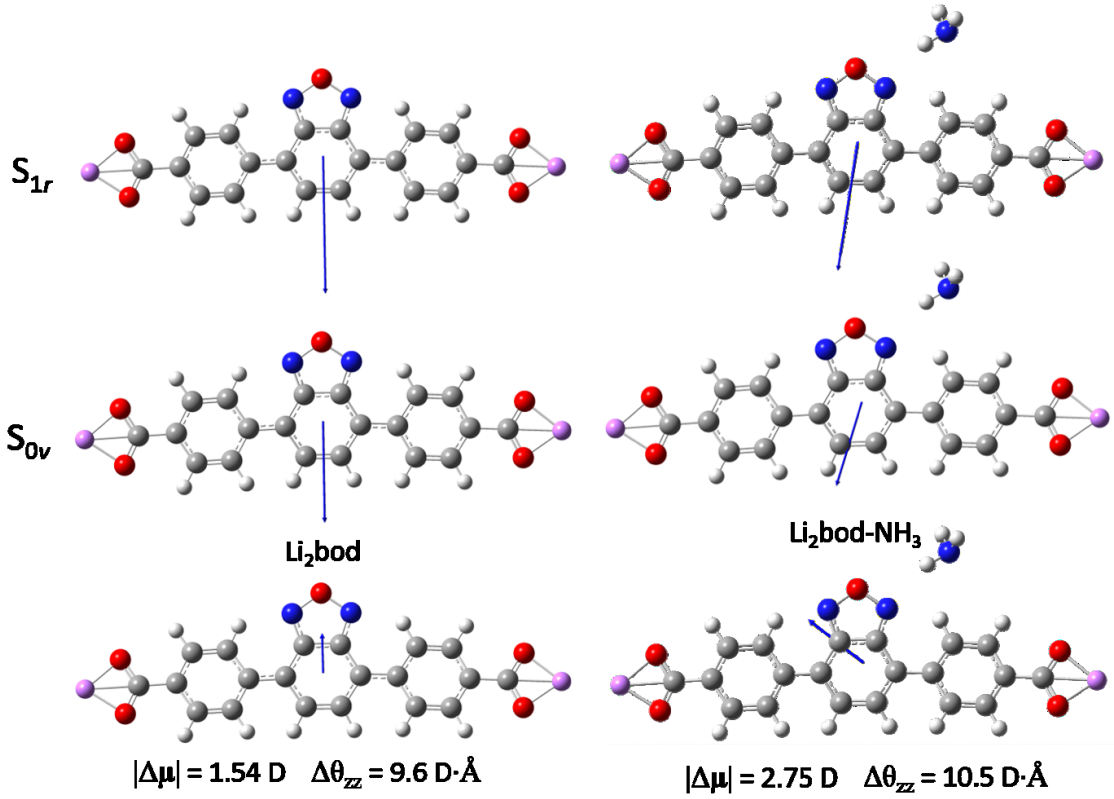

Figure S36. Optimised geometries (B3LYP 6-311+G(2d,p) of the first singlet excited states and vertical ground states for Li_2bod and Li_2bod-NH_3. Arrows indicate the electric dipole moments (for S_{1r} and S_{0v} states) or dipole moment difference vectors calculated from ESP atomic charges at CAM-B3LYP aug-cc-pVTZ level of theory.

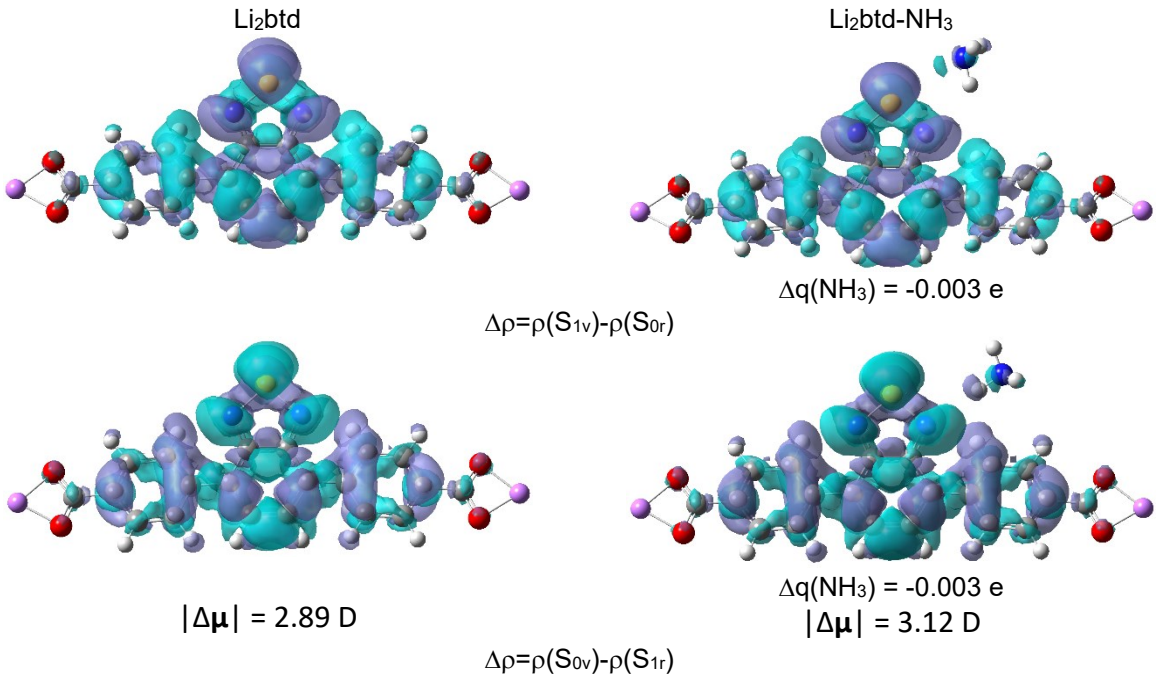

Figure S37. Isosurfaces (0.0004 $e^{1/2}/Bohr^{3/2}$) of electron density difference and changes of the sum of ESP atomic charges on NH_3 molecule for absorption and emission processes of Li_2btd and Li_2btd-NH_3 calculated CAM-B3LYP aug-cc-pVTZ level of theory.

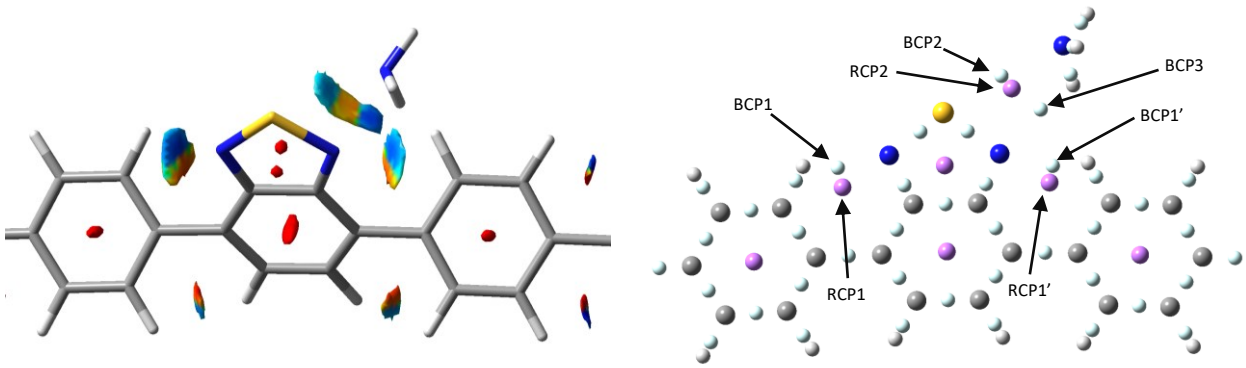

(a) (b)

Figure S38. Plot of the (a) Reduced Density Gradient (RDG) isosurfaces (isovalue *s* = ½) and (b) the Critical Points (CPs). Colour scale: -0.012 a.u. (blue; strong attraction) ≤ sign(λ_2)ρ(**r**) ≤ +0. 012 a.u. (red; strong repulsion). Legend of colours: white (H), grey (C), blue (N), red (O), light blue (Bond CPs), and mauve (Ring CPs).

Table S1. Dependence of missing linker defect content in UiO-68(bod) synthesised using different modulators.

Modulator used	Mass of the sample (mg)	Mass of the internal standard (mg)	Calculated mass of the linkers (mg)	Mass % of the organic part	Defect content
Benzoic acid	4.9	1.0	3.06	62.3	1 missing linker per Zr cluster
Formic acid	5.2	1.0	3.39	65.2	0.8 missing linkers per 1 Zr cluster
L-proline	4.8	1.0	3.07	63.9	0.9 missing linkers per 1 Zr cluster

Table S2. MOFs sensitive towards ammonia in the gas and aqueous phase.

MOF	Measured property	LOD, ppm	Reference
detection in the gas phase			
$\{Na[Cd(MIDC)]\}_n$	electrical conductance	0.05	[2]
NDC-Y-fcu-MOF	capacitance	0.10	[3]
NiPc-Ni	electrical resistance	0.31	[4]
NiPc-Cu	electrical resistance	0.33	[4]
$Cu_3(HITP)_2$	electrical resistance	0.5	[5]
EC-MOF, $Cu_3(HHTP)_2$	electrical resistance	0.5	[6]
$Ba(o\text{-}CbPhH_2IDC)(H_2O)_4]_n$	electrical impedance	1	[7]
FJU-56	UV-Vis absorbance	1.38	[8]
[Cu(p-IPhHIDC)]n	electrical impedance	2	[9]
Eu^{3+}@Ga(OH)bpydc	luminescence quenching	2.4	[10]
SNNU-88	electrical resistance	~5	[11]
ZA-MPTMS-Eu-UiO-67	luminescence quenching	8.4	[12]
Zn(NA)	electrical resistance	10	[13]
ZnO@ZIF-71	electrical resistance	~10	[14]
ZnO@ZIF-8	electrical resistance	~10	[14]
BG/Ti3CN, $Fe^{III}Fe^{III}(CN)_6$	electrical resistance	~10	[15]
MR-MOF-Eu	luminescence quenching	10.8	[16]
CuBTC	electrical resistance	20	[17]
MIL-124@Eu^{3+}	luminescence	26	[18]
SION-10	UV-Vis absorbance	300	[19]
$Mg(H_2DHBDC)$	luminescence turn on	n/d	[20]
Cu-TCPP-on-Cu-HHTP	electrical resistance	n/d	[21]
detection in water			
UiO-68(bod)	**luminescence turn on**	**0.0065**	**this work**
$[(TabH)(AgBr_2)]_n$	electrical resistance	0.05	[22]
SNNU-88	luminescence quenching	~1.5	[11]
$\{[Cd_4(HIDCPy)_6]\cdot 4DMF\cdot 4C_2H_8N\cdot H_2O\}_n$	luminescence turn on	n/d	[23]

Table S3. Calculated values of total electron density (ρ), Lagrangian and Hamiltonian kinetic energies (G and K, respectively), potential energy (V), energy density (H), Laplacian of the total density (Δρ), Electron Localisation Function (ELF), Source Function (SF), total electrostatic potential (ESP), ellipticity of the total electron density (ε) and eta index (η), computed at the selected Bond (BCPs) and Ring Critical Points (RCPs) in $[Li_2bod\cdot NH_3]$

CP	ρ(r)	G(r)	K(r)	V(r)	H(r)	Δρ(r)	ELF(r)	SF(r)	ESP(r)	ε[ρ(r)]	η(r)
BCP1	1.03698E-02	7.79435E-03	-1.80888E-03	-5.98547E-03	1.80888E-03	3.84129E-02	3.18643E-02	-5.32549E-04	2.43987E-02	0.10584	0.14678
BCP1'	8.84061E-03	6.67404E-03	-1.55313E-03	-5.12091E-03	1.55313E-03	3.29087E-02	2.56861E-02	-5.08461E-04	1.94219E-02	0.18227	0.13335
BCP2	6.18936E-03	4.03620E-03	-8.18837E-04	-3.21736E-03	8.18837E-04	1.94202E-02	2.14508E-02	-1.96408E-04	-1.74174E-02	0.40834	0.17940
BCP3	9.83665E-03	6.40158E-03	-1.37776E-03	-5.02382E-03	1.37776E-03	3.11173E-02	3.92908E-02	-3.57670E-04	2.51890E-02	0.07872	0.19637
RCP1	8.84064E-03	8.76426E-03	-2.53484E-03	-6.22943E-03	2.53484E-03	4.51964E-02	1.50684E-02	-7.14882E-04	6.08382E-02	-1.38990	0.10493
RCP1'	8.16101E-03	7.69276E-03	-2.20342E-03	-5.48934E-03	2.20342E-03	3.95847E-02	1.49774E-02	-6.94319E-04	4.96256E-02	-1.46787	0.09581
RCP2	4.36520E-03	3.35556E-03	-7.93277E-04	-2.56228E-03	7.93277E-04	1.65953E-02	9.79703E-03	-1.96159E-04	-6.36057E-03	-1.47358	0.24475

Table S4. Calculated values of total electron density (ρ), Lagrangian and Hamiltonian kinetic energies (G and K, respectively), potential energy (V), energy density (H), Laplacian of the total density (Δρ), Electron Localisation Function (ELF), Source Function (SF), total electrostatic potential (ESP), ellipticity of the total electron density (ε) and eta index (η), computed at the selected Bond (BCPs) and Ring Critical Points (RCPs) in [Li_2bod·NH_3]

CP	ρ(r)	G(r)	K(r)	V(r)	H(r)	Δρ(r)	ELF(r)	SF(r)	ESP(r)	ε[ρ(r)]	η(r)
BCP1	1.01057E-02	7.50555E-03	-1.83786E-03	-5.66770E-03	1.83786E-03	3.73736E-02	3.15389E-02	-5.32976E-04	2.15058E-03	0.34348	0.14346
BCP1'	9.53062E-03	7.13787E-03	-1.75396E-03	-5.38391E-03	1.75396E-03	3.55673E-02	2.87638E-02	-5.54492E-04	5.42029E-03	0.47632	0.13427
BCP2	7.84715E-03	5.08882E-03	-9.07508E-04	-4.18131E-03	9.07508E-04	2.39853E-02	2.95491E-02	-2.45654E-04	3.94306E-03	0.66699	0.15485
BCP3	9.99592E-03	7.05451E-03	-1.51371E-03	-5.54079E-03	1.51371E-03	3.42729E-02	3.43201E-02	-3.89015E-04	1.13657E-02	0.33925	0.18070
RCP1	9.26362E-03	8.87520E-03	-2.44046E-03	-6.43474E-03	2.44046E-03	4.52626E-02	1.71355E-02	-7.14805E-04	2.95670E-02	-1.44257	0.09006
RCP1'	9.05974E-03	8.37518E-03	-2.29125E-03	-6.08393E-03	2.29125E-03	4.26658E-02	1.78515E-02	-7.33382E-04	2.77696E-02	-1.54330	0.08481
RCP2	7.56213E-03	5.79131E-03	-1.20663E-03	-4.58468E-03	1.20663E-03	2.79918E-02	2.03686E-02	-3.03527E-04	1.42192E-02	-2.61134	0.16235

References

1 A. Monge, J. A. Palop, A. L. de Cerain, V. Senador, F. J. Martinez, Y. Sainz, S. Narro, E. Garcia and C. de Miguel, *J. Med. Chem.*, 1995, **38**, 1786–1792.

2 R. Liu, Y. Liu, S. Yu, C. Yang, Z. Li and G. Li, *ACS Appl. Mater. Interfaces*, 2019, **11**, 1713–1722.

3 A. H. Assen, O. Yassine, O. Shekhah, M. Eddaoudi and K. N. Salama, *ACS Sensors*, 2017, **2**, 1294–1301.

4 Z. Meng, A. Aykanat and K. A. Mirica, *J. Am. Chem. Soc.*, 2019, **141**, 2046–2053.

5 M. G. Campbell, D. Sheberla, S. F. Liu, T. M. Swager and M. Dincă, *Angew. Chemie Int. Ed.*, 2015, **54**, 4349–4352.

6 M.-S. Yao, X.-J. Lv, Z.-H. Fu, W.-H. Li, W.-H. Deng, G.-D. Wu and G. Xu, *Angew. Chemie Int. Ed.*, 2017, **56**, 16510–16514.

7 K. Guo, L. Zhao, S. Yu, W. Zhou, Z. Li and G. Li, *Inorg. Chem.*, 2018, **57**, 7104–7112.

8 J. Zhang, J. Ouyang, Y. Ye, Z. Li, Q. Lin, T. Chen, Z. Zhang and S. Xiang, *ACS Appl. Mater. Interfaces*, 2018, **10**, 27465–27471.

9 Z. Sun, S. Yu, L. Zhao, J. Wang, Z. Li and G. Li, *Chem. – A Eur. J.*, 2018, **24**, 10829–10839.

10 J.-N. Hao and B. Yan, *Nanoscale*, 2016, **8**, 2881–2886.

11 Y.-P. Li, S.-N. Li, Y.-C. Jiang, M.-C. Hu and Q.-G. Zhai, *Chem. Commun.*, 2018, **54**, 9789–9792.

12 J. Ma and B. Yan, *Spectrochim. Acta Part A Mol. Biomol. Spectrosc.*, 2019, **220**, 117107.

13 A. J. Mohan Reddy, N. K. Katari, P. Nagaraju and S. Manabolu Surya, *Mater. Chem. Phys.*, 2020, **241**, 122357.

14 T. Zhou, Y. Sang, X. Wang, C. Wu, D. Zeng and C. Xie, *Sensors Actuators B Chem.*, 2018, **258**, 1099–1106.

15 T. Yang, L. Gao, W. Wang, J. Kang, G. Zhao, D. Li, W. Chen and H. Zhang, *Nano-Micro Lett.*, 2021, **13**, 63.

16 J. Ma, L.-M. Zhao, C.-Y. Jin and B. Yan, *Dye. Pigment.*, 2020, **173**, 107883.

17 H. Spieser, Z. Tehrani, M. M. Ali, E. D. Ahmadi, A. Denneulin, J. Bras, D. Deganello and D. Gethin, *J. Mater. Chem. C*, 2021, **9**, 6332–6343.

18 J. Zhang, D. Yue, T. Xia, Y. Cui, Y. Yang and G. Qian, *Microporous Mesoporous Mater.*, 2017, **253**, 146–150.

19 A. Gładysiak, T. N. Nguyen, J. A. R. Navarro, M. J. Rosseinsky and K. C. Stylianou, *Chem. – A Eur. J.*, 2017, **23**, 13602–13606.

20 N. B. Shustova, A. F. Cozzolino, S. Reineke, M. Baldo and M. Dincă, *J. Am. Chem. Soc.*, 2013, **135**, 13326–13329.

21 M.-S. Yao, J.-W. Xiu, Q.-Q. Huang, W.-H. Li, W.-W. Wu, A.-Q. Wu, L.-A. Cao, W.-H. Deng, G.-E. Wang and G. Xu, *Angew. Chemie Int. Ed.*, 2019, **58**, 14915–14919.

22 F. Wang, Y.-T. Wang, H. Yu, J.-X. Chen, B.-B. Gao and J.-P. Lang, *Inorg. Chem.*, 2016, **55**, 9417–9423.

23 J. Ma, T. Zhou, T. Ma, Z. Yang, J.-H. Yang, Q. Guo, W. Liu, Q. Yang, W. Liu and T. Yang, *Cryst. Growth Des.*, 2021, **21**, 383–395.